# Internal Structure Analysis of Polypropylene/Quartz Composites Related to Their Toughness

**Ezequiel Pérez,**[1,2] **Celina Bernal,**[3] **Claudio Javier Pérez**[4]
[1]*National Council for Scientific and Technical Research (CONICET), Buenos Aires, Argentina*

[2]*Plastics Research and Development Center, National Institute of Industrial Technology (INTI-Plásticos), Av. Gral. Paz 5445 e/ Constituyentes y Albarellos, (B1650KNA), San Martín, Buenos Aires, Argentina*

[3]*Institute of Polymers Technology and Nanotechnology, ITPN (UBA-CONICET), Engineering Faculty, University of Buenos Aires, Av. Las Heras 2214 (C1127AAR), Buenos Aires, Argentina*

[4]*Polymer Science and Engineering Group, Research Institute of Material Science and Technology (INTEMA)—National University of Mar del Plata (UNMdP), Av. Juan B. Justo 4302, (7600) Mar del Plata, Argentina*

**The mechanical performance of composite materials has been related to a wide range of factors. The complexity of analysis lays on the fact that any single variation normally affects many characteristics or properties of the composite material. For this reason, different theoretical and experimental characterizations should be considered. In this work the internal structure, interactions and fracture surfaces of PP-based composites reinforced with quartz particles are investigated. Particle size distributions, rheological measurements and multifractal spectra suggest favorable filler dispersion into the PP matrix. A yield strength model and rheological data evidence low internal interactions. In addition, these composites characteristics could promote the effective activation of energy consumption mechanisms improving the material toughness. The fracture surfaces analysis allows correlating fractography, multifractal spectra and material toughness. However, the experimental procedure of multifractal theory should be improved to define the most sensitive parameter for fractographic studies. POLYM. COMPOS., 37:1488–1496, 2016.** **© 2014 Society of Plastics Engineers**

## INTRODUCTION

Composite materials mechanical properties have been related to several kinds of factors that can be briefly listed as: components properties and interactions, filler content and size, internal structures, among others [1–3]. It could be really complex to analyze the effect of these parameters on the mechanical performance due to any single variation normally affects many different characteristics of the composite material [4–7]. As example: smaller particle size or larger filler contents can improve the composite material fracture toughness. On the other hand, these variations could increase the filler aggregation probability [3, 4, 8–10]. Processing optimization (method and parameters) promotes favorable filler dispersion due to increased shear forces, but it could be detrimental for the matrix properties related to thermo-mechanical degradation [11–13].

The study of matrix properties, internal structures and interactions (filler/filler and matrix/filler) represent a quite relevant topic for understanding of polymer based composite properties [6, 9, 14–17]. In addition, the fracture surface analysis bring significant information about failure and energy release processes [7, 18–21]. Nowadays, different theoretical and experimental tools (micrographic observations, rheological measurements, fractal and multifractal theories, models for predicting mechanical properties, numerical simulations, among others) are used to investigate these characteristics and phenomena [15, 19, 22–27]. Unfortunately, any of them can easily explain the effect of a defined parameter (matrix characteristics, morphology, etc.) on the composite properties. For this reason, each performed analysis should be compared and complemented with other ones.

The aim of this work was to analyze the internal structure, interactions and morphology of fracture surfaces of Polypropylene/quartz composite materials. Morphological

*Correspondence to*: E. Pérez; e-mail: eperez@inti.gob.ar
Contract grant sponsor: National Research Council of Argentina (CONICET)..
DOI 10.1002/pc.23318
Published online in Wiley Online Library (wileyonlinelibrary.com).
© 2014 Society of Plastics Engineers

and rheological analyses were performed. A tensile strength model was considered, particle size distributions, and multifractal spectra were determined.

## EXPERIMENTAL

### *Composite Materials*

A commercial polypropylene (PP) homopolymer (PP1102H, melt flow index 1.8 g/10 min) provided by Petroquímica Cuyo (Argentina) was used as the matrix of the composites. Quartz particles were used as reinforcement with contents of: 5, 10, 20, 30, 40 wt% of raw particle and 2.5, 5 wt% of milled particle in an attrition milling for 16 h. The composites were called as: PP-filler content r/m, where the letters (r, m) mean raw or milled quartz, respectively. PP matrix and composites were blended in an intensive mixer at 190°C and 50 r.p.m. for 10 min. The different blends were compression molded in a hydraulic press at 180°C and a pressure of 100 kPa for 10 min to obtain sheets of nominal thickness 1 mm. The sheets were cooled by water within the press under constant pressure.

### *Mechanical Tests*

**Tensile Tests.** A universal testing machine (INSTRON 1125) was used for uniaxial tensile tests at a crosshead speed of 5 mm $min^{-1}$ following standard recommendations (ASTM D638). Tensile parameters values were originally published [28].

**Impact Tests.** Izod impact tests were carried out with a Custom Scientific Instruments Inc. (CS-137D-177) according to ASTM D 256. For each analyzed material, five samples were tested at least. The results were originally published [28].

**Internal Structure Analysis.** Different theoretical and experimental tools were applied to analyze the internal structure and interactions of the composite materials as detailed below.

**Morphology.** Scanning electron microscopy (SEM) micrographs were obtained for the quartz particles and fracture surfaces of tested samples at 2,500× and 5,000× magnifications. Samples had been coated with a thin layer of gold and observed in a FEI QUANTA 250.

**Particle Size Distribution.** Particle size distributions were obtained for the filler before blending and within the different composites. A commercial software (*ImageJ*) was used to measure the particles maximal length on SEM micrographs. A minimum of 300 particles were analyzed in each case to warrant statistical validity.

**Rheology.** An Anton Paar Rheometer MCR301 (small amplitude oscillatory shear flow between parallel plates of 25 mm) was used for rheological measurements under a nitrogen atmosphere at 190°C in the frequency range of 0.1–500 $s^{-1}$. The samples used ($Ø = 25$ mm and 1 mm thickness) were cut from the compression molded sheets. Dynamic strain sweeps were also performed to determine the linear strain range of each material. The rheological data was analyzed by Cole–Cole diagram and van Gurp–Palmen diagram.

To plot the Cole–Cole diagram $\eta''$ vs. $\eta'$ should be represented. A perfect arc means the absence of higher order structures and the relaxation behavior corresponds to a single relaxation time. The presence of a tail, a second arc or an increased correlation evidences structural changes or the presence of an internal structure (agglomeration, skeleton, house-of-cards structure, among others). The flattening of the curve is related to a relaxation time spectrum [9, 29]. To plot the van Gurp–Palmen diagram the phase angle ($\delta$) vs. the absolute complex modulus ($G^*$) should be represented ($\delta = \text{atan}(G''/G')$ and $|G^*| = (G'^2 + G''^2)^{1/2}$). This diagram is used to analyze the composite morphology stability or the applicability of the time-temperature superposition (TTS) principle [23, 29]. A microstructure, increased interactions or rheological percolation threshold can be detected by a shift of the curve or its shape variation [30, 31].

**Tensile Yield Stress Model.** The model proposed by Pukánszky et al. was used to predict the tensile yield stress of composite materials as a filler function. Basically, the model assumed that this property is related to matrix yield stress, effective load bearing capability and components interaction [25, 32]:

$$\sigma_y = \sigma_{y0}(1 - v_f)/(1 + 2.5v_f)\exp(Bv_f) \quad (1)$$

where $\sigma_y$ composite yield stress, $\sigma_{y0}$ matrix yield stress, $v_f$ filler volume fraction and $B$ a parameter related to the load-bearing capacity of the filler. The natural logarithm of reduced form should be plotted:

$$\ln(\sigma_{yred}) = \ln\left(\frac{\sigma_y}{\sigma_{y0}}(1 + 2.5v_f)/(1 - v_f)\right) = Bv_f \quad (2)$$

Deviations from a linear fitting mean the presence of internal structures while the slope of the straight line ($B$ parameter value) is related to the matrix/filler interaction [25].

**Multifractal Theory.** The multifractal theory was considered to analyze the filler dispersion and the fractography of tested samples. The spectra were calculated by the box counting method based on SEM images. More detailed information about the multifractal theory and its experimental procedure can be found in the references [19, 27, 33]. Briefly, a global image for each material should be obtained and covered with boxes of variable length ($\varepsilon$). The grid reduction allows analyzing the

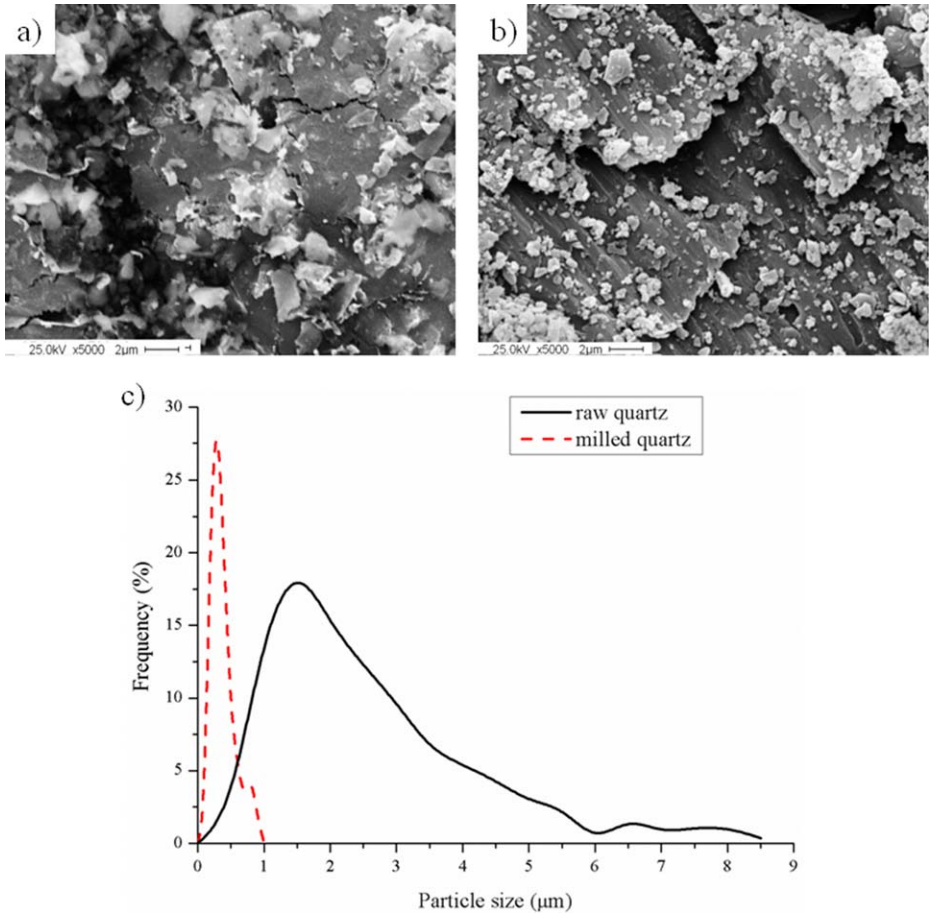


FIG. 1. SEM micrographs of (a) raw quartz, (b) milled quartz, and (c) particle size distribution. [Color figure can be viewed in the online issue, which is available at wileyonlinelibrary.com.]

scaling range of the multifractal phenomena [34]. The following definition of measure was considered:

$$\mu_{ij}(\varepsilon)=\frac{n_{ij}}{\sum n_{ij}} \tag{3}$$

For filler dispersion and morphological analysis the quantity of particles and the mean gray value distribution were used as measured parameter, respectively. The considered $\mu_{ij}$ (ε) can be described in a multifractal spectrum as follows:

$$\mu_{ij}(\varepsilon) \propto \varepsilon^{\alpha} \tag{4}$$

$$N_{\alpha}(\varepsilon) \propto \varepsilon^{-f(\alpha)} \tag{5}$$

where $N_\alpha$ number of boxes with the same α value. The α-concentration of a box is the log/log version of a measure per unit of length:

$$\alpha(\varepsilon)=\frac{\log(\mu_{ij}(\varepsilon))}{\log(\varepsilon)} \tag{6}$$

Finally, the $f(\alpha)$ values represent the fractal dimension of α–concentration subsets:

$$f(\alpha)=\frac{\log(N_{\alpha})}{\log(\varepsilon)} \tag{7}$$

MATLAB™ codes were developed to obtain the corresponding multifractal spectra for filler dispersion and fracture surface morphology analysis diminishing possible experimental mistakes. The accuracy of proposed algorithms was warranted comparing their results with data previously published [19].

## RESULTS AND DISCUSSION

The internal structures and interactions of PP/quartz composites were analyzed, discussed and related to material toughness.

### *Morphological Analysis*

Raw and milled quartz particles used as fillers are shown in Fig. 1. Morphological observations and particle size distributions suggest an effective milling process (milled particle lengths were clearly smaller than raw quartz dimensions). In addition, specific surface area measurements ($4.5 \pm 0.3$ $m^2$ $g^{-1}$ and $18.5 \pm 0.3$ $m^2$ $g^{-1}$

 DOI 10.1002/pc

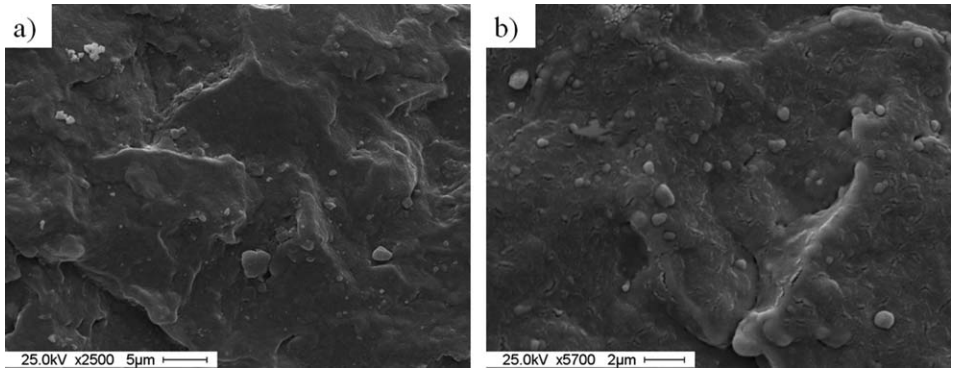


FIG. 2. SEM micrographs of cryo-fractured surfaces: (a) PP-5r and (b) PP-5m.

for raw and milled quartz, respectively) confirmed this observation.

For the different composites, a homogeneous morphology was detected. For instance, composite materials with 5 wt% of raw and milled quartz (Fig. 2) displayed a good filler dispersion and agglomerates were only locally observed. This kind of morphology represents a favorable internal structure capable to effectively activate energy absorption mechanisms (debonding of particles, plastic void growth, matrix yielding, multiple crazing, among others) [7, 18, 35–37].

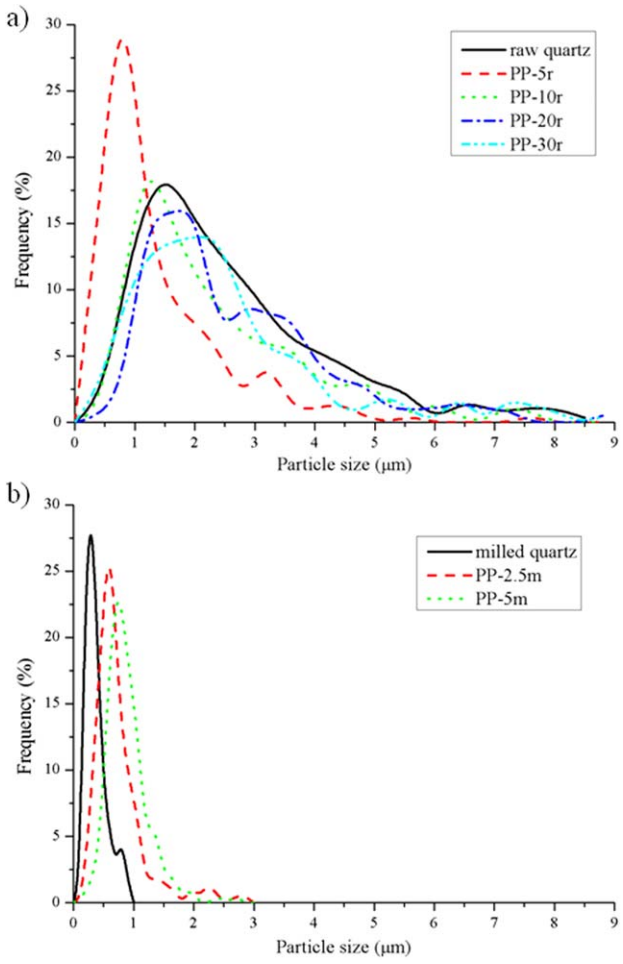


FIG. 3. Particle size distribution for filler and composites: (a) PP-r and (b) PP-m. [Color figure can be viewed in the online issue, which is available at wileyonlinelibrary.com.]

*Particle Size Distribution Analysis*

Particle size distributions were determined for raw and milled quartz before blending and also for the particles within the PP matrix. Only distinguishable particles were considered for filler distributions. On the other hand, for composite materials both individual particles and agglomerates were measured. Particle size distribution within the PP-5r composite (Fig. 3a) displayed a narrower distribution with a shift lo lower values of the most frequent size, compared to raw particle distribution, and a tail at larger length. For increased filler contents, irregular and broader distributions were observed. All distributions (raw quartz before blending and within composites) displayed similar size values. In addition, for the PP-r composites the peaks at large sizes can be related to the simultaneous presence of largest particles and agglomerates.

Milled quartz distributions (Fig. 3b) exhibited considerable lower values, compared to raw filler. The PP-m systems, compared to milled filler, displayed broader distributions with increased most frequent sizes. For these materials, the peaks observed at large length values can be related, exclusively, to filler agglomerates due to milled particles exhibited considerable smaller sizes.

*Rheological Analysis*

The Cole-Cole diagrams for PP-r and PP-m composites are plotted in Fig. 4. A perfect arc can be identified for the PP matrix and the PP-r composites (Fig. 4a) suggesting the absence of any significant structural change with filler content. On the other hand, the tail detected for the PP-30r composite corresponds to filler aggregation [9, 14]. In a similar way, for the PP-m systems (Fig. 4b) any structural modification was detected varying the filler

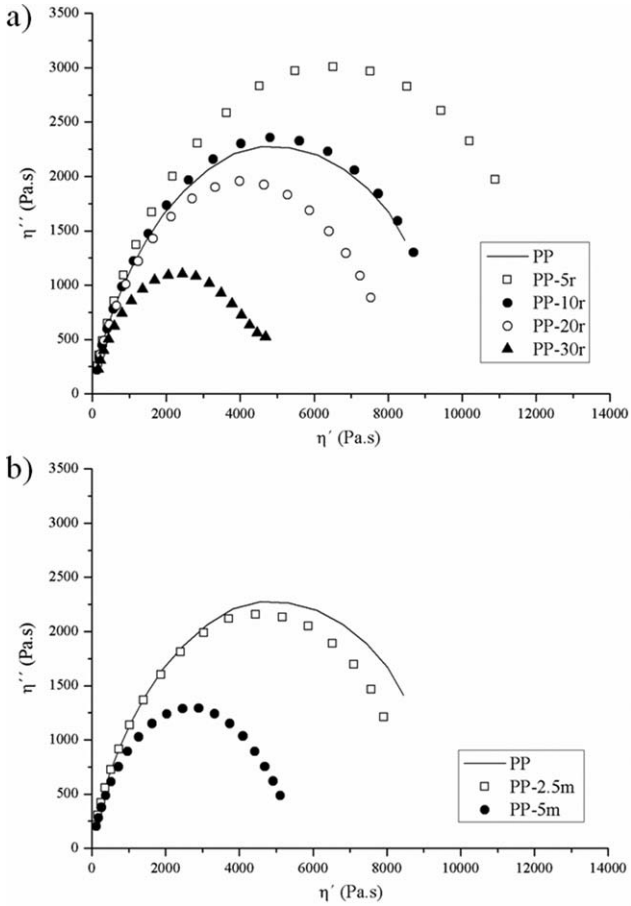


FIG. 4. Cole–Cole plots for: (a) PP-r and (b) PP-m.

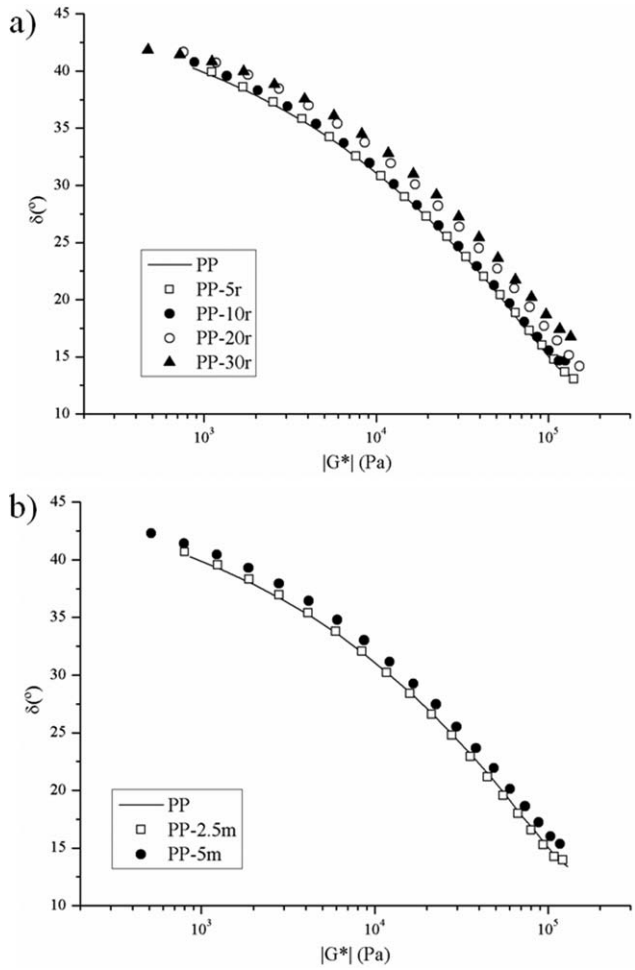


FIG. 5. Van Gurp-Palmen plots for: (a) PP-r and (b) PP-m.

content. Decreased curve areas were probably related to polymer degradation. In addition, it has been reported that PP degradation does not affect the Cole–Cole curve shape [38].

The corresponding van Gurp–Palmen diagrams for the analyzed materials are plotted in Fig. 5. In general, similar curves were detected for the PP matrix and the composites suggesting a stable internal structure independently of the filler content and size. The absence of a percolation threshold could be explained by a weak filler/filler interaction [23, 39]. On the other hand, it has been reported repulsive effects between fillers for z-potential values greater than +30 mv or lower than −30 mv [40]. Z-potential measurements confirmed a repulsive effect for quartz particles (−37.6 ± 0.8 mv).

### *Tensile Yield Stress Model Analysis*

To apply the model proposed by Pukánszky et al. a linear correlation of the reduced yield stress vs. filler volume fraction should be found (Fig. 6). For PP-r and PP-m systems the corresponding slopes were roughly horizontal related to a weak filler/matrix interaction [25, 32]. In addition, internal structure variations with filler content could not be analyzed by this model.

### *Multifractal Analysis*

Filler dispersion and fractography were analyzed by multifractal theory. Figure 7 shows SEM micrographs used for both analysis and correspond to the fracture

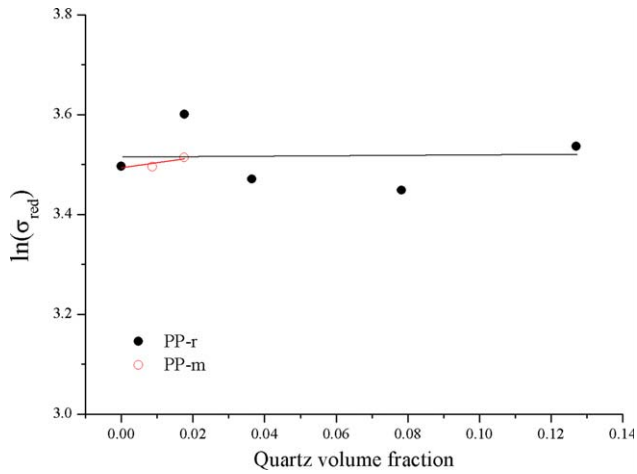


FIG. 6. Tensile yield stress model for PP-r and PP-m composites. [Color figure can be viewed in the online issue, which is available at wileyonlinelibrary.com.]

 DOI 10.1002/pc

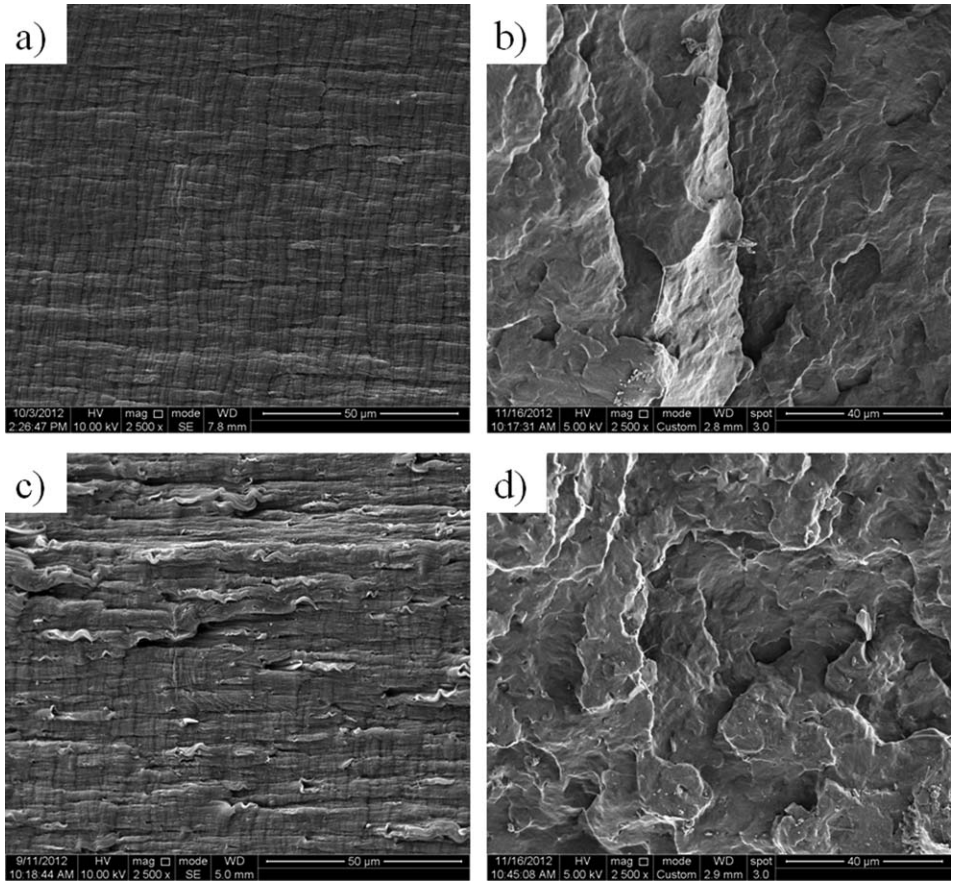


FIG. 7. Fracture surfaces of: (a) PP tensile test, (b) PP impact test, (c) PP-2.5m tensile test, and (d) PP-2.5m impact test.

surfaces of PP matrix and PP-2.5m composite broken in tensile and impact tests, as examples.

*Filler Dispersion Analysis*

Initially, the scaling range was analyzed obtaining similar values to previously reported by others authors [34]. The corresponding linear regression (Fig. 8a) for the PP-10r composite confirms the applicability of multifractal theory. Similar plots were obtained for all of the studied materials (not shown here). The multifractal spectra for the PP-r composites (Fig. 8b and Table 1) displayed almost constant $\alpha_{min}$ values related to largest agglomerate sizes. On the other hand, the shift of $\alpha(f_{max})$ values evidence a larger most frequent agglomerate size. Variations of $\alpha_{max}$ values suggest an increment of the smaller agglomerates sizes with a reduction of isolated particles number. For the PP-m composites (Fig. 8c and Table 1), the spectra shift to lower values evidence larger agglomerate sizes distribution. It should also be highlight that similar tendencies were observed for the PP-r and PP-m systems by morphological and particle size distribution analysis.

*Fracture Surfaces Analysis*

The mean gray value distribution was considered as the measured parameter to characterize the fracture surfaces. The obtained linear plot (scaling range) for the PP-10r composite (Fig. 9a) indicates the applicability of the multifractal theory for this kind of analysis. The determined linear range was similar to all of the studied materials. For samples broken in tensile tests, the spectra general trends (Fig. 9b and 9c and Table 2) displayed a reduction of $\alpha_{max}$ values with filler content variation related to lower material toughness [27, 41, 42]. On the other hand, the $\alpha_{min}$ values remained almost constant for all analyzed materials. Figure 10 shows the corresponding spectra for samples of PP matrix and PP-m composites broken in impacts tests. In a similar way the most important spectra variations were found at large $\alpha$ values.

*Multifractal Spectra Related to Material Toughness*

For the PP-r systems, similar trends of $\Delta\alpha$ and tensile toughness values were observed (Fig. 11a). This suggests that the multifractal experimental procedure is able to analyze the fracture surfaces morphology of analyzed composites. This kind of relationships between multifractal parameters and mechanical properties have been already reported for similar materials [27, 41]. On the other hand, taking into account the PP matrix tensile toughness, a spectrum with maximal values ($\alpha_{max}$ and $\Delta\alpha$) should be expected. However, this kind of spectrum was

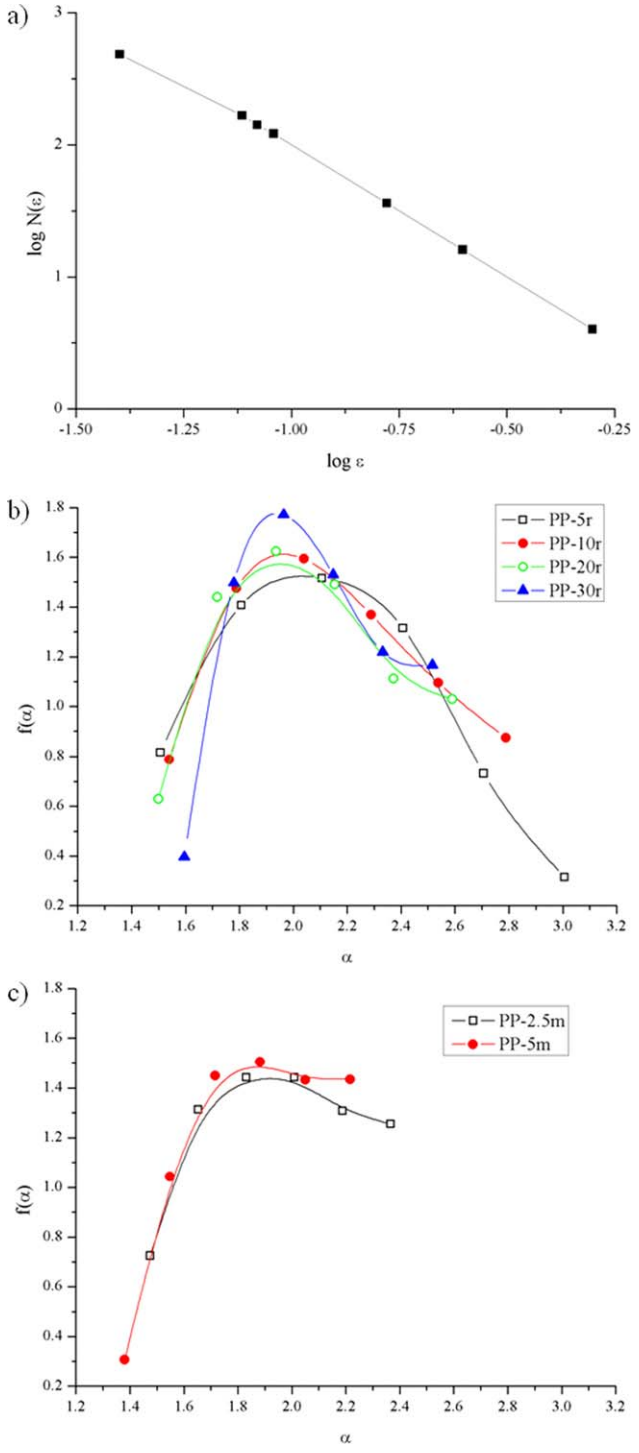


FIG. 8. Multifractal analysis of filler dispersion: (a) scaling range, (b) PP-r spectra, and (c) PP-m spectra. [Color figure can be viewed in the online issue, which is available at wileyonlinelibrary.com.]

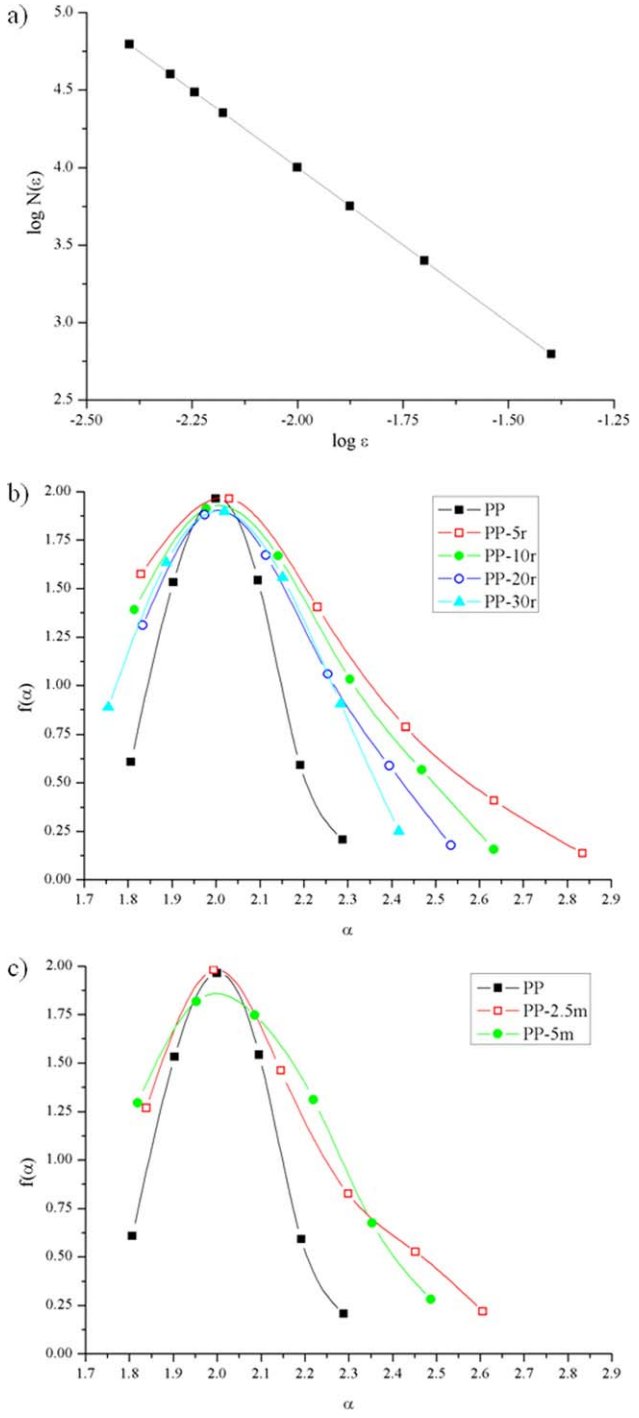


FIG. 9. Multifractal analysis of tensile fracture surfaces: (a) scaling range, (b) PP- r spectra, and (c) PP-m spectra. [Color figure can be viewed in the online issue, which is available at wileyonlinelibrary.com.]

not detected in this work. This unexpected behavior could be explained by the presence of quartz particles that influence the experimental results. The corresponding gray value distributions for the matrix and particles were simultaneously measured, affecting the fracture surfaces spectra. For impact tests similar trends of toughness and $\Delta\alpha$ values were observed, for the matrix and PP-m composites (Fig. 11b), suggesting a negligible effect on the gray value distribution. These results indicated a more significant influence for irregular surfaces, qualitatively analyzed by comparison of the gray distributions for ductile surface, brittle surface and filler. This experimental limitation could be overcome by comparing each material itself with different surface morphologies. That means,

 DOI 10.1002/pc

TABLE 1. Multifractal spectra parameters for filler dispersion analysis.

| | $\alpha_{min}$ | $\alpha_{max}$ | $\Delta\alpha$ | $f(\alpha_{min})$ | $f(\alpha_{max})$ | $\Delta f(\alpha)$ |
|---|---|---|---|---|---|---|
| | | | **PP-r** | | | |
| PP-5r | 1.5062 | 3.0062 | 1.5000 | 0.8154 | 0.3154 | 0.5000 |
| PP-10r | 1.5393 | 2.7882 | 1.2488 | 0.7879 | 0.8725 | −0.0845 |
| PP-20r | 1.4996 | 2.589 | 1.0894 | 0.6295 | 1.0281 | −0.3986 |
| PP-30r | 1.5952 | 2.5158 | 0.9206 | 0.3964 | 1.1662 | −0.7697 |
| | | | **PP-m** | | | |
| PP-2.5m | 1.4745 | 2.3659 | 0.8915 | 0.7245 | 1.25517 | −0.53064 |
| PP-5m | 1.3807 | 2.2167 | 0.8359 | 0.3065 | 1.43481 | −1.12824 |

the spectrum of a fully brittle surface (e.g., cryo-fractured) can be taken as a reference in comparison with fracture surfaces. Finally, another possible limitation of experimental procedure lays on the measured parameter. Is the mean gray value distribution the most sensitive parameter for fractography analysis? For example, if we compare the spectra for samples of the PP matrix broken in tensile and impact tests. Based on the more brittle behavior exhibited by the matrix under impact loading condition, a narrower spectrum could be expected. But the opposite tendency was observed and this behavior cannot be related to the particle presence.

## CONCLUSIONS

The internal structure, interactions and morphology of fracture surfaces of PP-based composites reinforced with quartz were investigated. In general, morphological observations and particle size distributions indicated favorable filler dispersion with localized agglomerates. In addition, rheological and multifractal studies confirmed these observations. On the other hand, low interactions were detected from the application of a yield stress model and rheological behavior. These kinds of morphologies and interactions can promote the effective activation of energy consumption mechanisms favoring the material toughness.

TABLE 2. Multifractal spectra parameters for fracture surfaces analysis.

| | $\alpha_{min}$ | $\alpha_{max}$ | $\Delta\alpha$ | $f(\alpha_{min})$ | $f(\alpha_{max})$ | $\Delta f(\alpha)$ |
|---|---|---|---|---|---|---|
| | | | **PP (tensile test)** | | | |
| PP | 1.8062 | 2.2882 | 0.4821 | 0.6075 | 0.2073 | 0.4002 |
| | | | **PP-r (tensile test)** | | | |
| PP-5r | 1.8286 | 2.8341 | 1.0054 | 1.5740 | 0.1366 | 1.4375 |
| PP-10r | 1.8138 | 2.6321 | 0.8182 | 1.3906 | 0.1582 | 1.2324 |
| PP-20r | 1.8334 | 2.5348 | 0.7014 | 1.3098 | 0.1772 | 1.1326 |
| PP-30r | 1.7545 | 2.4164 | 0.6618 | 0.8881 | 0.2507 | 0.6374 |
| | | | **PP-m (tensile test)** | | | |
| PP-2.5m | 1.8381 | 2.605 | 0.7675 | 1.2685 | 0.2193 | 1.0493 |
| PP-5m | 1.8181 | 2.4872 | 0.6691 | 1.2941 | 0.2808 | 1.0133 |
| | | | **PP-m (impact test)** | | | |
| PP | 1.8519 | 2.5292 | 0.6773 | 1.5366 | 0.1693 | 1.3673 |
| PP-2.5m | 1.8282 | 2.4034 | 0.5752 | 0.907 | 0.1692 | 0.7378 |
| PP-5m | 1.8256 | 2.7081 | 0.8825 | 1.4997 | 0.1631 | 1.3366 |

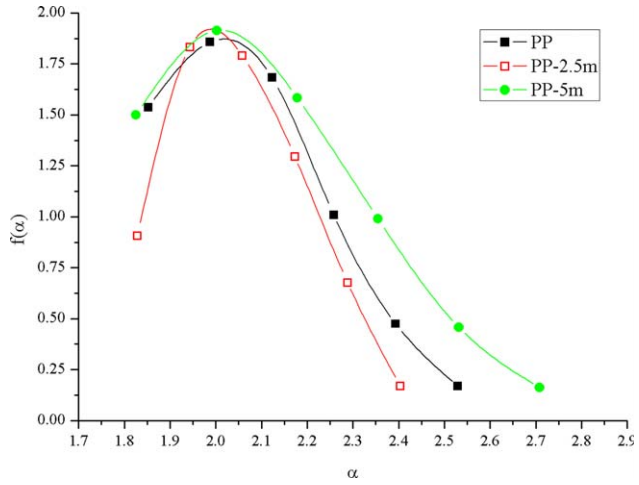


FIG. 10. Multifractal analysis of impact fracture surfaces of PP-m composite. [Color figure can be viewed in the online issue, which is available at wileyonlinelibrary.com.]

Fracture surfaces analysis allowed to establish a correlation between multifractal spectra and material toughness values. However, experimental limitations related to the filler presence and to the limited sensitive of measured

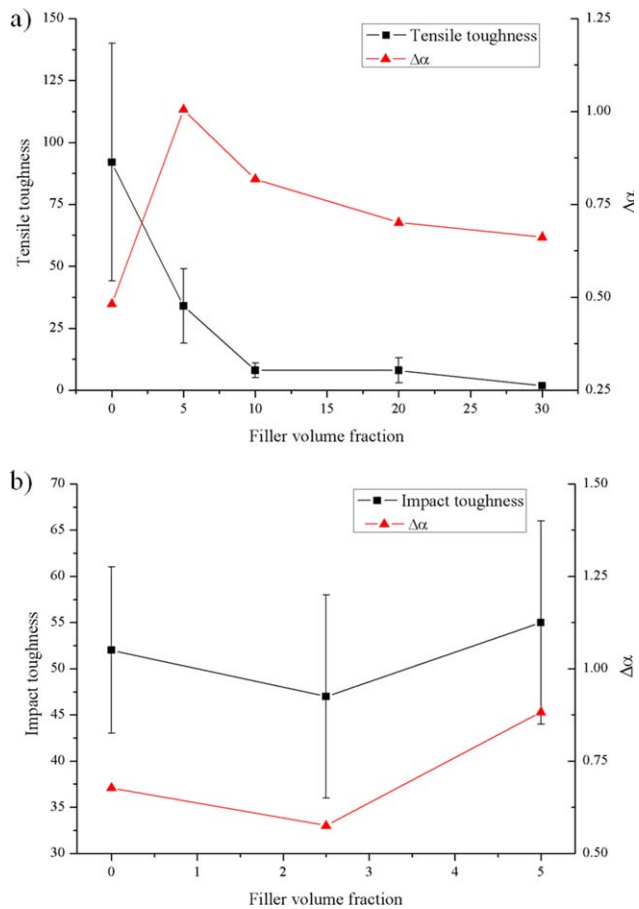


FIG. 11. Multifractal spectra width related to: (a) tensile toughness and (b) impact toughness. [Color figure can be viewed in the online issue, which is available at wileyonlinelibrary.com.]

parameter were found. Discussion and definition of the most sensitive parameter for fractographic analysis is still needed.

## ACKNOWLEDGMENTS

The authors thank Prof. M. Piacquadio and G. Dutt for their helpful comments and for introducing us into the interesting world of fractal theory and their science applications and to Prof. L. Fasce for her useful comments and discussions about multifractal experimental procedure.

## REFERENCES

1. Z. Bartczak, A.S. Argon, R.E. Cohen, and M. Weinberg, *Polymer*, **40**, 2347 (1999).
2. A. Galeski, *Prog. Polym. Sci*., **28**, 1643 (2003).
3. J. Móczo and B. Pukánszky, *Ind. Eng. Chem*., **14**, 535 (2008).
4. S.-Y. Fu, X.-Q. Feng, B. Lauke, and Y.-W. Mai, *Compos. B*, **39**, 933 (2008).
5. E. Pérez, V. Alvarez, C.J. Pérez, and C. Bernal, *Compos. B*, **52**, 72 (2013).
6. T. Sun, F. Chen, X. Dong, and C.C. Han, *Polymer*, **49**, 2717 (2008).
7. B. Cotterell, J.Y.H. Chia, and K. Hbaieb, *Eng. Fract. Mech*., **74**, 1054 (2007).
8. R. Dangtungee, J. Yun, and P. Supaphol, *Polym. Test*., **24**, 2 (2005).
9. A. Kiss, E. Fekete, and B. Pukánszky, *Comp. Sci. Tech*., **67**, 1574 (2007).
10. L. Sun, R.F. Gibson, F. Gordaninejad, and J. Suhr, *Comp. Sci. Tech*., **69**, 2392 (2009).
11. G. Guerrica-Echevarría, J.I. Eguiazábal, and J. Nazábal, *Polym. Degrad. Stabil*., **53**, 1 (1996).
12. W. Camacho and S. Karlsson, *Polym. Degrad. Stabil*., **78**, 385 (2002).
13. Z. Dominkovics, J. Hári, E. Fekete, and B. Pukánszky, *Polym. Degrad. Stabil*., **96**, 581 (2011).
14. Á. Ábranyi, L. Százdi, B. Pukánszky Jr., G.J. Vancsó, and B. Pukánszky, *Macromol. Rapid Commun*., **27**, 132 (2006).
15. M. Okamoto, P.H. Nam, P. Maiti, T. Kotaka, N. Hasegawa, and A. Usuki, *Nano Lett*., **1**(**6**), 295 (2001).
16. B. Fayolle, A. Tcharkhtchi, and J. Verdu, *Polym. Test*., **23**, 939 (2004).
17. D. Bertin, M. Leblanc, S.R.A. Marque, and D. Sir, *Polym. Degrad. Stabil*., **95**, 782 (2010).
18. R.A.C. Deblieck, D.J.M. van Beek, K. Remerie, and I.M. Ward, *Polymer*, **52**, 2979 (2011).
19. E. Pérez, C. Bernal, and M. Piacquadio, *Appl. Surf. Sci*., **258**, 8940 (2012).
20. V. Shah, *Handbook of Plastics Testing and Failure Analysis*, Wiley, New Jersey (2007).
21. A.B. Martinez, J. Gamez-Perez, M. Sanchez-Soto, J.I. Velasco JI, O.O. Santana, and M.L. Maspoch, *Eng. Fail. Anal*., **16**, 2604 (2009).
22. J.Z. Liang, *Comp. A*, **38**, 1502 (2007).
23. P. Reichert, B. Hoffmann, B. Thorsten, R. Thomann, R. Mülhaupt, and C. Friedrich, *Macromol. Rapid. Commun*., **22**, 519 (2001).
24. X.-L. Xie, Q.-X. Liu, R.K. Li, X.-P. Zhou, Q.-X. Zhang, Z.-Z. Yu, and Y.-W. Mai, *Polymer*, **45**, 6665 (2004).
25. L. Százdi, A. Pozsgay, and B. Pukánszky, *Eur. Polym*., **43**, 345 (2007).
26. B. Lauke and S.-Y. Fu, *Comp. B*, **45**, 1569 (2013).
27. Y.-H. Zhang, B.-F. Baib, J.-Q. Li, J.-B. Chen, and C.-Y. Shen, *App. Surf. Sci*., **257**, 2984 (2011).
28. E. Pérez, *Development of Composite Materials Based on Polypropylene Reinforced With Rigid Particles*, University of Buenos Aires, Buenos Aires (2014).
29. J. Ahmed, R. Auras, T. Kijchavengkul, and S.K. Varshney, *Food Eng*., **111**, 580 (2012).
30. O. Meincke, D. Kaempfer, H. Weickmann, C. Friedrich, M. Vathauer, and H. Warth, *Polymer*, **45**, 739 (2004).
31. O. Valentino, M. Sarno, N.G. Rainone, M.R. Nobile, P. Ciambelli, H.C. Neitzert, and G.P. Simon, *Phys. E*, **40**, 2440 (2008).
32. L. Százdi, B. Pukánszky Jr., G.J. Vancso, and B. Pukánszky, *Polymer*, **47**, 4638 (2006).
33. M. Rosen and M. Piacquadio, Math. Ph., arXiv:0804.3426v2 (2008).
34. O. Malcai, D.A. Lidar, O. Biham, and D. Avnir, *Phys. Rev. E*, **56**, 2817 (1997).
35. J.G. Williams, *Comp. Sci. Tech*., **70**, 885 (2010).
36. W.C.J. Zuiderduin, C. Westzaan, J. Huetink, and R.J. Gaymans, *Polymer*, **44**(**1**), 261 (2003).
37. J. Móczó, *Particulate Filled Polymers: Interaction, Structure and Micromechanical Deformations*, Budapest University of Technology and Economics, Budapest (2004).
38. H. Azizi, I. Ghasemi, and M. Karrabi, *Polym. Test*., **27**, 548 (2008).
39. A.K. Barick and D.K. Tripathy, *Appl. Clay. Sci*., **52**, 312 (2011).
40. D.B. Genovese and J.E. Lozano, *Food Hyd*., **15**, 1 (2001).
41. Y.-H. Zhang, B.-F. Bai, J.-B. Chen, C.-Y. Shen, and J.-Q. Li, *Appl. Surf. Sci*., **256**, 7151 (2010).
42. E. Pérez, C.J. Pérez, V.A. Alvarez, and C. Bernal, *Carbohyd. Polym*., **97**, 269 (2013).